

Tuning Ionic Screening To Accelerate Electrochemical CO₂ Reduction in Ionic Liquid Electrolytes

Beichen Liu, Wenxiao Guo, and Matthew A. Gebbie*


 Cite This: *ACS Catal.* 2022, 12, 9706–9716


Read Online

ACCESS |

Metrics & More

Article Recommendations

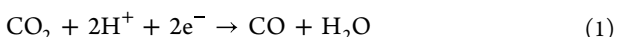
Supporting Information

ABSTRACT: Electric double layer formation often governs the rate and selectivity of CO₂ electrochemical reduction. Ionic correlations critically define double layer properties that are essential to electrocatalytic performance, including capacitance and localization of potential gradients. However, the influence of ionic correlations on CO₂ electroreduction remains unexplored. Here, we use electrochemical conversion of CO₂ to CO in ionic liquid-based electrolytes to investigate how the emergence of ionic correlations with increasing ion concentration influences reaction rates and selectivity. Remarkably, we find substantial acceleration of potential-dependent CO₂ reduction rates and enhancement of faradaic efficiency to CO at intermediate concentrations of 0.9 M ionic liquid in acetonitrile, a concentration regime that has not been studied previously. We find that onset potentials for CO₂ reduction remain relatively unchanged at -2.01 V vs Ag/Ag⁺ from 0.025 M up to 1.1 M and increase to -2.04 V vs Ag/Ag⁺ in the limit of neat ionic liquids. Hence, the acceleration of CO₂ reduction we observe originates from the amplification of potential-dependent driving forces, as opposed to changes in onset potential. Importantly, our findings are general across cocatalytic and noncatalytic ions. We propose that concentrations of maximum reactivity correspond to conditions where electric double layers exhibit the strongest screening, which would localize electric fields to stabilize polar intermediates. Our study demonstrates that tuning bulk electrostatic screening lengths via modulation of ionic clustering provides a general approach to accelerating both inner-sphere and outer-sphere electrochemical reactions.

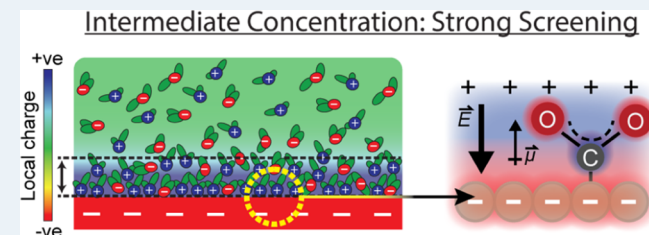
KEYWORDS: *electrocatalysis, ionic liquids, electric double layer, interfaces, electrochemistry*

INTRODUCTION

Electrochemical reduction of CO₂ to CO and other products could provide opportunities to minimize the carbon footprints of industrial processes by replacing fossil fuels with waste or atmospheric CO₂. Conversion of CO₂ proceeds via mechanisms where the first step often involves a two proton, two-electron half-reaction to convert CO₂ into CO (eq 1), usually through the formation of a negative radical intermediate,^{1,2} which can then further react to wide-ranging products. Notably, the concurrent generation of H₂ by the hydrogen evolution reaction (HER) also occurs via a two proton, two-electron half-reaction at similar, often lower, onset potentials, particularly in aqueous solutions. Hence, a key challenge for the implementation of electrochemical CO₂ reduction is to devise approaches to favor CO₂ reduction, while simultaneously inhibiting electron flow into the HER pathway.



Recently, chemical modulation of electrolyte properties, such as the inclusion of cations that stabilize CO₂ reduction transition states, has emerged as an important tool in tipping the balance away from the HER and toward CO₂ reduction.^{3–7} For example, ionic liquid-based electrolytes where cations are designed to selectively coordinate CO₂ have emerged as



promising cocatalytic promoters of selective electroreduction of CO₂ to CO.^{3,6–10}

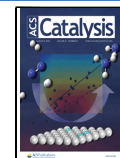
Ionic liquids are salts typically composed of bulky organic cations combined with a variety of anions, which may be organic or inorganic.^{11–13} While neat ionic liquids exhibit advantageous properties for CO₂ electroreduction, including high electrochemical stability, CO₂ solubility, and intrinsic ionic conductivity, they are too viscous to facilitate high current densities needed for practical processes. As a result, ionic liquids are often blended into aqueous and nonaqueous solutions when implemented in electrocatalytic studies.

Cocatalysis of CO₂ reduction via ionic liquids was first demonstrated by Rosen and co-workers, where aqueous electrolytes with ion concentrations of 4.26 M were used in combination with silver electrodes.³ This study showed that dialkyl imidazolium cations could serve as cocatalysts for CO₂ reduction at unprecedentedly low onset potentials for selective

Received: May 2, 2022

Revised: July 10, 2022

Published: July 26, 2022



reduction of CO_2 to CO , despite the presence of large amounts of water. Subsequent publications delved into possible mechanisms for HER suppression and enhancement of CO_2 reduction.^{4–6} Leading possibilities for enhancement of CO_2 reduction include cation hydrogen-bond stabilization of transition states^{14–16} and carbene-mediated coordination of CO_2 via cation complexes to activate CO_2 .^{14,17–22} HER suppression mechanisms are typically centered around exclusion of water from interfaces.^{7,23}

Despite initial reports by Rosen and colleagues of pronounced enhancement of CO_2 reduction in aqueous electrolytes with very high ion concentrations, subsequent studies proceeded to focus on understanding how ion molecular structures influence CO_2 reduction in either neat ionic liquids or low-concentration ionic liquid-supporting electrolyte blends. Dilute and neat ionic liquid electrolytes appear to be emphasized because dilute electrolytes maximize CO_2 transport due to low solution viscosity and neat ionic liquids maximize CO_2 solubility. For cases when ionic liquids are blended with solvent, acetonitrile has emerged as a common choice because of its low viscosity, large electrochemical window, and high CO_2 solubility.²⁴

Nonetheless, current mechanistic understandings of ionic liquid-mediated CO_2 electrochemical reduction focus more on molecular interactions between single ionic liquid ions and CO_2 , while the influence of collective ion correlations and self-assembly on reactivity is often overlooked. Critically, current investigations appear to avoid intermediate concentrations, especially as ion concentrations begin to exceed dilute limits, which is around 1 M for an aqueous solution. For less polar solvents, such as acetonitrile, this crossover is shifted to lower concentrations.²⁵ Notably, this is the regime where ionic correlations are expected to emerge.

Therefore, we designed a systematic study of CO_2 reduction in ionic liquid solutions at varying concentrations, with a focus on intermediate concentrations, to illuminate the role of ionic correlations in electrochemical reactivity. Given that many electrochemical devices use electrolytes with ion concentrations that exceed the dilute limit, such insights will have broad implications that extend beyond CO_2 electrolysis processes.

Our core hypothesis is that ionic liquid-mediated CO_2 electrochemical reduction rates will exhibit nonmonotonic scaling with electrolyte ion concentration and will be maximized at intermediate concentrations. Electrochemical reaction rates and pathways are closely related to the properties of electric double layers. Our hypothesis builds on recent findings from the surface force community showing that electric double layers often exhibit the most efficient screening, as evidenced by minimized electrostatic screening lengths, at intermediate concentrations, compared with dilute solution and high concentrations.^{26–31} These observations stand in contrast to the classical Debye–Hückel theory, which predicts that increasing ion concentrations systematically increases the efficiency of electrostatic screening by decreasing screening lengths.

The nonmonotonic relationship between ion concentrations and electrostatic screening lengths was interpreted as an indication that ionic correlations and clustering begin to emerge at high ion concentrations and that correlations cause many dissolved ions to become “bound” in effectively neutral aggregates.^{26,27,32} This formation of aggregates reduces the population of “free” ions available to screen charged surfaces.

As a result, electric double layers that form in highly concentrated electrolytes are much thicker, or less efficiently screened, than would be predicted via frameworks, like Debye–Hückel theory, which assumes that ions are independently “free” to screen electrodes.^{25–27,30,31,33} Tuning ionic correlations by varying ion concentration should influence many properties of electrode–electrolyte interfaces that dictate electrocatalytic reactivity.^{34–38}

We thus envision that the modulation of ionic correlations via concentration would allow us to achieve enhanced electrostatic screening, which would aid in breaking bonds and stabilizing transition states through localizing electric field gradients to electrode surfaces. Here, we describe our proof-of-concept study of how ion correlations and screening can be used as a complementary method for controlling electrochemical reactions. We chose the electroreduction of CO_2 to CO on silver electrodes in ionic liquid/acetonitrile blends with controlled water concentrations of 900–1100 ppm as our model reaction to illustrate how a holistic approach of considering double layer formation at electrocatalytic interfaces can qualitatively transform common reactivity metrics.

Our findings demonstrate that ionic strength can alter reactivity in ways that can rival the influence of the specific chemical structures of the ionic liquid ions studied. We used electrochemical kinetics approaches, including cyclic voltammetry (CV) measurements, to conduct ion concentration sweeps and reveal nonmonotonic enhancement of CO_2 electroreduction rates for both cocatalytic and noncatalytic ionic liquid-based electrolytes (Figure 1). We then performed chronoamperometry (CA) and product analysis studies (Figure 2) to show that steady-state current densities and faradaic efficiencies (FEs) reflect enhanced kinetics measured at intermediate concentrations. To gain insight into the mechanisms of this rate enhancement, we performed in situ electrochemical surface-enhanced Raman scattering (SERS) spectroscopy studies, which provide clues suggesting that rate acceleration originates in the enhancement of local potential gradients at concentrations that yield maximum current densities and FEs (Figure 3).

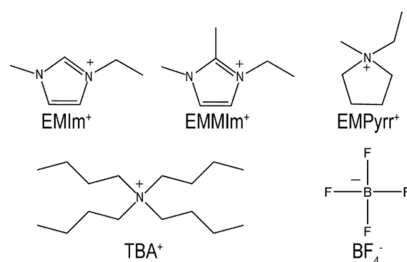
Finally, we describe a noteworthy case where increases in ion concentration ultimately lead to cathode passivation through the formation of (bi)carbonate resulting from the reaction between CO_2 and OH^- (Figure 4). This provides key insight into the role of the imidazolium ionic liquid in enhancing CO_2 reduction rates, suggesting new strategies for mitigating electrode passivation in organic electrolytes.

RESULTS

Cyclic Voltammetry. We first analyzed the electrochemical behavior of ionic liquid solutions of varying concentrations separately under Ar- and CO_2 -saturated solution conditions. Using 1-ethyl-3-methylimidazolium tetrafluoroborate (EMIm BF_4^-) in combination with a common supporting electrolyte salt tetrabutylammonium tetrafluoroborate (TBA BF_4^-) (Scheme 1), we examined ionic liquid-derived electrolytes with ions dissolved in acetonitrile at low concentrations that are commonly described in the literature. We observed CV results in agreement with prior studies for 25 mM EMIm BF_4^- containing 0.1 M TBA BF_4^- and neat EMIm BF_4^- (Figure 1A).^{14,19,35,39–41}

Presenting the same data but with the molar fraction of EMIm BF_4^- rather than concentration produces a very similar graph (Figure S1) and does not change our observations and

Scheme 1. Chemical Structures of Ionic Liquid Cations and Anions Used in This Work



conclusions. We choose to present our findings as a function of ion concentration, which is an indication of the density of ions per unit volume. Ion density is a key metric describing the emergence of ion clustering and assembly, which occurs at ionic densities that bring neighboring ions to separation distances smaller than the Bjerrum length.²⁷ In contrast, the molar fraction requires separately accounting for size discrepancies between cations, anions, and solvents to determine when correlations emerge.

We then studied how the chemical structures of ions influence interfacial properties. Interestingly, the CV response of 125 mM EMIm BF₄ solution was comparable to that of 25 mM EMIm BF₄ + 0.1 M TBA BF₄ solution, exhibiting very similar onset potentials and current densities. Onset potentials are dictated by charge transfer activation energies, while current densities provide an indication of reaction rates.

Typically, EMIm BF₄ is thought to be a cocatalyst for the CO₂ electroreduction reaction, while TBA BF₄ is used as a supporting electrolyte to mitigate solution resistance losses. If the cocatalytic nature of EMIm BF₄ is critical at these lower solution concentrations, then electrolytes with higher concentrations of EMIm BF₄ should yield higher current densities. The similarities in both onset potential and current density suggest that the total ion concentration has a larger influence on reactivity than the identity of the dissolved cations in the low-concentration regime. Within the low-concentration regime for these electrolytes, we conclude that CO₂ reduction is largely independent of specific ion properties but is instead

proceeding via an outer-sphere mechanism or direct electrode-CO₂ electron transfer.

Another notable finding from our work is that the onset potentials and current densities measured for neat EMIm BF₄ and the dilute (25 mM, no TBA BF₄) EMIm BF₄ solutions are similar. This surprising result, which is also observed for EMPyrr BF₄ and TBA BF₄ (Figures S4 and S6), raises the possibility that reaction environments exhibited by some neat liquids may share analogies to reaction environments present in dilute electrolyte solutions, as ion clustering can dramatically suppress the availability of “free ions” to screen charged surfaces and localize potential gradients. Such an interpretation is consistent with discussions from the surface force community, where it is proposed that large electrostatic screening lengths present in ionic liquids cause them to behave analogously to dilute electrolytes, where very few “free” ions are available to redistribute and screen charged surfaces.^{25,26,30,33}

Most importantly, we observed a remarkable increase in CO₂ reduction rates, in the form of enhanced current densities, as we increased the concentration of EMIm BF₄. At intermediate concentrations, such as 0.5 M EMIm BF₄ (Figure 1A), we observed current densities that were almost double that of more dilute concentrations. Such high current densities were absent when electrolytes were purged with Ar (Figure S2). Notably, onset potentials for CO₂ reduction did not vary greatly within this intermediate-concentration regime. Hence, our concentration-dependent measurements indicate that the activation energy for the CO₂ reduction reaction is similar across varying concentrations, but the reaction rate was substantially enhanced at intermediate concentration, as compared to the dilute and neat concentrations.

Small differences in onset potentials may be observed if an iR correction is used to account for solution resistance potential drops, where there is an associated potential drop required for current to flow in an electrochemical cell. In electrolytes with low conductivity, the potential experienced by reactants and products at the working electrode can be much smaller in magnitude than the potential applied by the potentiostat and resulting voltammetry curves would appear linear rather than exponential with an increase in potential due

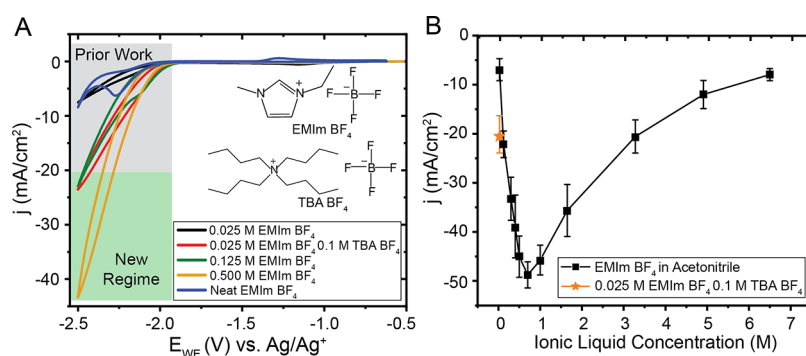


Figure 1. Nonmonotonic concentration-dependent reactivity of CO₂ electrochemical reduction in CO₂-saturated acetonitrile solutions of EMIm BF₄ at varying concentrations. (A) Representative CV results. Compared to the dilute and neat ionic liquid limits typically used in electrocatalysis studies, intermediate concentrations display a significant increase in current densities from CO₂ electrochemical reduction. (B) Nonmonotonic concentration dependence of current densities. At -2.5 V vs Ag/Ag⁺, we observe pronounced increases in reactivity at intermediate concentrations of EMIm BF₄ in acetonitrile. Using the current densities at -2.5 V vs Ag/Ag⁺ as a representative value for a relatively high polarization, we find a remarkable average current density of 48.6 ± 3.0 mA/cm² at 0.7 M EMIm BF₄, which is more than double that of more traditional concentrations, such as neat EMIm BF₄ or 25 mM EMIm BF₄ + 0.1 M TBA BF₄. Each data point and error bar represents three independent trials, from which two representative CVs were used for each trial for a total of at least six values.

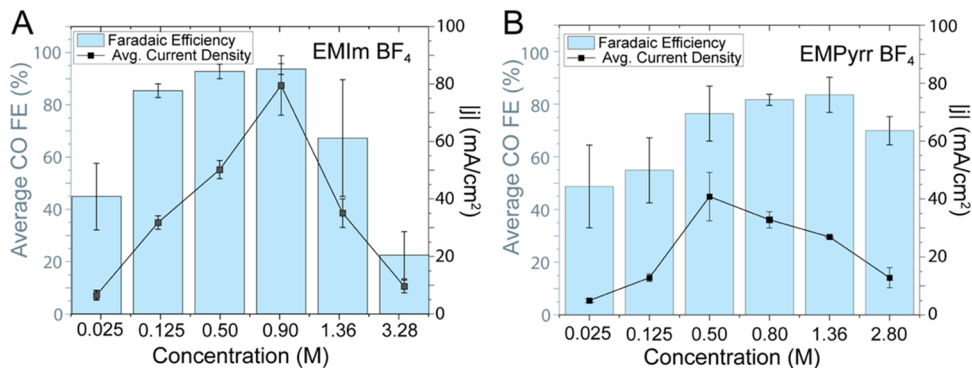


Figure 2. Steady-state FEs for CO production and current densities (j) obtained over the course of hours 1–3 of CA at -2.5 V vs Ag/Ag^+ on Ag electrodes for varying concentrations of (A) EMIm BF_4 and (B) EMPyrr BF_4 in acetonitrile solvent. While EMIm BF_4 displayed higher steady-state current densities and FEs at intermediate concentrations, EMIm BF_4 and EMPyrr BF_4 share a similar nonmonotonic enhancement of both current densities and FEs along with concentrations, suggesting that this enhancement is not ion-specific. Each data point represents an average and standard deviation obtained from seven time points collected for each sample.

to solution resistance.⁴² As seen in Figure 1, the key intermediate-concentration regimes that are the focus of our work exhibit CV curves that are more exponential in nature than linear, and accounting for iR drops would further increase the pronounced rate enhancement we observed.

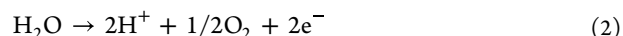
Nevertheless, the 25 mM and neat EMIm BF_4 electrolytes do exhibit characteristics of solution resistance-limited rates (Figure 1A), indicating that solution resistance plays a larger role at these two extreme concentrations. Solution resistance is dependent on cell geometry, so we maintained consistent distances and orientations between working and reference electrodes for all experiments.⁴² To account for the solution resistance component of CV measurements, an iR correction can be applied, where a solution resistance-related potential drop is calculated or measured and subtracted from the reported potential. When this data transformation is implemented, CV curves appear exponential. We present the untransformed data in the main text as we found that applying iR corrections will not change the trends and key features that we observe and present in this work.

In addition to solution conductivity, the identity of the proton donor involved in CO_2 reduction can have a large influence on reaction rates. In many cases, water is the only proton donor available to participate in CO_2 reduction, particularly when water is doped into aprotic solvents, like acetonitrile. In EMIm BF_4 solutions, imidazolium cations can also donate the acidic two-site proton, which can cause EMIm cations to become the primary proton donor in intermediate-to-high concentration solution studied here. Future work evaluating how water concentration and the presence or absence of proton donors other than water influences reactivity would be illuminating in light of the universal enhancement of reaction rate with ion concentration we report here.

Overall, we conclude that changes in solution resistance and water activity are unlikely to be primary reasons for the rate enhancements we observe. By keeping the initial concentration of the water constant among samples, we see variations in current density and FEs solely through changing cation structures (Figures 1, S4 and S6). If water activity or solution resistance was the dominant factor, we would expect to observe reactivity that was largely independent of the cation structure. Notably, our results support recent studies in the field, which increasingly suggest that cations play a leading role in determining CO_2 reduction activity^{5,43–45} and the likelihood

that water activity or solution resistance could have higher order effects on observed reactivity would complement our key findings and conclusions.

We also note that rigorous discussion of overpotentials for practical electrolysis using a complete electrochemical cell necessitates an understanding of both the cathodic and anodic reactions of interest. Conventionally, the cathodic reaction is depicted in eq 1, where CO_2 , two protons, and two electrons react to form CO and H_2O . The corresponding anodic reaction, particularly in aqueous electrolytes, is the oxidation of water into two protons and one oxygen atom (eq 2).



Using these two half-reactions, the overall thermodynamic potential is -1.33 V.^{3,46} As written, water should be neither generated nor consumed between the two half-reactions. During our trials, we observed a consistent increase in water content in the anolyte after CA, suggesting that the circuit was completed by anodic reactions other than water oxidation.^{16,47} Prior studies indicate that -1.5 V vs Ag/Ag^+ is the onset potential for the cathodic reaction shown in eq 1 in acetonitrile solutions of ionic liquids,⁴⁷ and we find this value to be the appropriate potential to use for calculating overpotentials. Taken together, we conclude that the onset potentials we report in this work are comparable to those in prior studies.

We then conducted a study in a wide concentration range of EMIm BF_4 with a particular focus on the intermediate concentrations. We observed a nonmonotonic enhancement of the reaction rate with concentration, with a maximum average current density of 0.7 M EMIm BF_4 (Figure 1B). CV is used primarily to study electrochemical reaction kinetics, so our results suggest that the maximum reaction rate enhancement of CO_2 reduction occurs at 0.7 M EMIm BF_4 . Beyond this concentration, however, the reactivity decreased such that current densities of the neat ionic liquid became similar to that of the 25 mM electrolyte.

Chronoamperometry. Figure 2 shows results from 3-hour-long electrolysis experiments under well-mixed conditions. Generally, the trends observed in CA experiments align well with the CV results. The steady-state current densities and corresponding FEs for CO reached a maximum at 0.9 M EMIm BF_4 rather than 0.7 M suggested by CV. In addition to CA experiments, we used nuclear magnetic resonance (NMR) to compare changes in the electrolyte

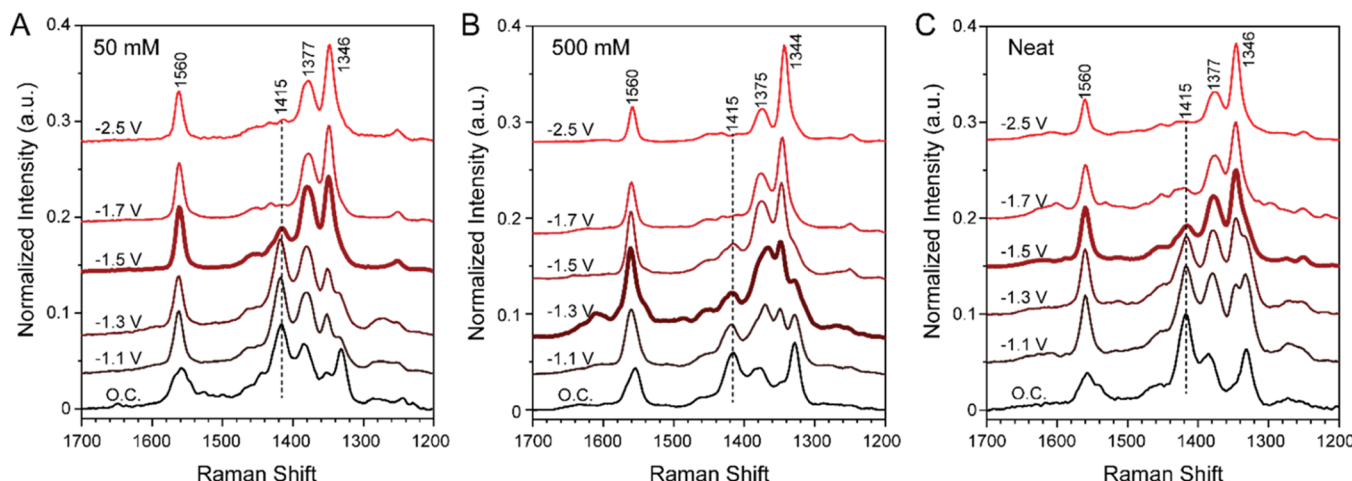
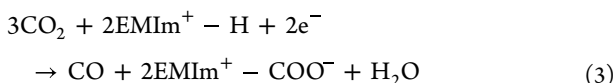


Figure 3. In situ SERS spectra of (A) 50 mM EMIm BF_4^- , (B) 500 mM EMIm BF_4^- , and (C) neat EMIm BF_4^- in the ring deformation region in forward potential sweeps. Intensities of peaks at 1560, 1375, and 1344 cm^{-1} gradually increase, and the peak at 1415 cm^{-1} gradually decreases when the potential is decreased from open-circuit potential to -2.5 V vs Ag/Ag^+ in all three cases (Figure S7). Nonetheless, the 500 mM EMIm BF_4^- exhibits more rapid changes in relative peak intensities compared with 50 mM and neat EMIm BF_4^- . While the intensity ratio of the 1344 cm^{-1} peak over the 1415 cm^{-1} peak is initially smaller than 1, it is inverted before the applied potential reaches -1.3 V for 500 mM EMIm BF_4^- . In contrast, at least -1.5 V was required to observe a similar inversion in the peak ratio for 50 mM and neat EMIm BF_4^- (Figure S10). At each concentration, the SERS spectrum from the potential required to invert the peak ratio between 1344 and 1415 cm^{-1} is bolded for a clearer comparison. O.C. stands for open-circuit potential (ca. -0.7 V vs Ag/Ag^+). In situ SERS spectra with the full wavenumber range and intermediate potential steps are shown in Figure S8.

composition before and after experiments. For EMIm BF_4^- , we observed formation of a carboxylate adduct in catholytes that has previously been reported in the literature.^{19,48,49} The abundance of this adduct was positively correlated with the current density of corresponding electrolytes and was the most pronounced in electrolytes with intermediate concentrations (Figure S3 and Table S1).

Reduction of CO_2 with water as the proton donor is known to generate HCO_3^- through the reaction between CO_2 and OH^- anions and is a major contributor to low FEs for CO_2 reduction reactions in alkaline or near-neutral pH media.^{43,50–52} Meanwhile, prior studies suggested that the carboxylate adduct spontaneously forms when EMIm cations and HCO_3^- coexist in acetonitrile.⁴⁷ We conclude that the formation of an adduct at the C2 position of the imidazolium cation ring in our study is more a byproduct of the reduction of CO_2 through the full reaction:



Indeed, the water content in catholytes increased by 1000 to 2000 ppm after 3-hour electrolysis, matching the trend predicted by the equation and suggesting that imidazolium cations serve as a primary proton donor for CO_2 reduction in EMIm BF_4^- electrolytes.

We observed a similar nonmonotonic trend in steady-state current densities and FEs for 1-ethyl-1-methylpyrrolidinium tetrafluoroborate (EMPyrr BF_4^-), an ionic liquid that is not considered a cocatalyst for CO_2 electroreduction and cannot act as a proton donor (Figure 2). In CA studies for EMPyrr BF_4^- , we found that the steady-state current densities and FEs reach a maximum at 0.5 M EMPyrr BF_4^- , instead of the maximum at 0.9 M observed for EMIm BF_4^- . Using CV, we measured the largest current densities for the 125 mM EMPyrr BF_4^- solution (Figure S4), which may be due to both the electrochemical cell setup and electrode cycling history. For

practical considerations, CA results are more directly applicable to electrolysis applications. NMR results indicated no significant change in the composition of the electrolyte after the electrolysis experiments (Figure S5).

In both EMIm BF_4^- and EMPyrr BF_4^- , acetonitrile decomposition accounts for the reduced FE at low concentrations⁵³ because H_2 production was absent and $^1\text{H}\text{NMR}$ showed similar impurity peaks for catholytes with different contents (Figures S3 and S5). At high concentrations, drops in steady-state current densities and FEs likely arise from ionic liquid decomposition^{41,49} because significant H_2 production was not observed, nor was the formation of carbonate species. Yet, due to the low current densities corresponding to these concentrations, ionic liquid decomposition products are not abundant enough to be detected by NMR of the bulk electrolyte.

We then tested the supporting electrolyte to further evaluate its role in the reduction reaction. CV trials with TBA BF_4^- exhibited very similar reactivity trends (Figure S6) to EMIm BF_4^- and EMPyrr BF_4^- , where the peak current density is achieved at concentrations lower than 1 M. Prior studies concluded that tetraalkylammonium-based salts are not cocatalysts for CO_2 electroreduction and mediate the reaction via an outer-sphere mechanism,^{24,54} which may explain the lower current densities for TBA BF_4^- when compared with EMIm BF_4^- .

Surface-Enhanced Raman Spectroscopy. With our observation of a concentration-dependent reactivity for TBA BF_4^- , we posit that the role of TBA BF_4^- both reduces solution resistance and impacts CO_2 electroreduction by influencing interfacial properties. The higher current densities and FEs we observed for EMIm BF_4^- still strongly point to imidazolium-based ionic liquids functioning as a cocatalyst, where the nonmonotonic behavior is amplified by the cocatalytic nature of EMIm cations. The nonmonotonic trend that we observe for both cocatalytic and noncatalytic ionic liquids provides evidence suggesting that this behavior is generalizable to

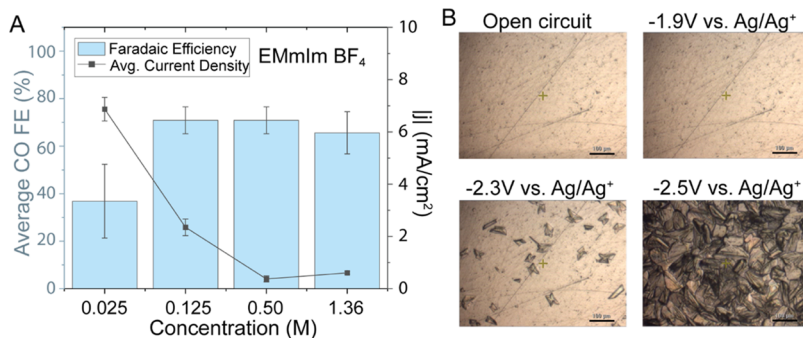


Figure 4. CA and FE results for CO₂-saturated acetonitrile solutions of EMImBF₄ at different concentrations and representative images of electrode passivation via the formation of EMImHCO₃. (A) CA and FE results. EMImBF₄ is considered a better cocatalyst than EMImBF₄ in previous literature at dilute concentrations. However, EMImBF₄ displays an unexpected decrease in steady-state current densities at concentrations beyond 125 mM, while faradaic efficiencies at these concentrations are near-constant. (B) Nucleation and growth of EMImHCO₃ crystals in a CO₂-saturated acetonitrile solution of 0.125 M EMImBF₄ at 10× magnification. Crystals started to form at potentials exceeding -2.3 V. These crystals likely limit mass transport of reactants and products across interfaces, accounting for the decrease in reactivity at relatively higher concentrations shown in (A). Interestingly, onset potentials for crystallization, crystal morphology, and crystal growth rate vary drastically with solution conditions (Figures S18–S21). Scale bars in (B) stand for 100 μm.

different ion structures. We propose that difference in electric potential gradients mediated by the collective assembly of ions is a likely mechanism influencing reactivity. Thus, we used *in situ* SERS to gain molecular-level insights into the potential-modulated assembly of ions in the electric double layer and determine how electric potential gradients depend on the concentration of ionic liquid ions (Figure 3).

For EMImBF₄ solutions, the intensity of SERS peaks at 1560, 1376, and 1344 cm⁻¹ in the imidazolium ring fingerprint region increase during cathodic potential sweeps,^{55,56} which is accompanied by a decrease in the intensity of a peak at 1415 cm⁻¹. Identical spectral changes occurred in both CO₂-saturated (Figure 3) and Ar-purged solutions (Figure S9), which can be interpreted as reorientation of EMIm⁺ in response to the electric fields.^{48,57} We use the intensity ratio of the peak at 1344 cm⁻¹ to the peak at 1415 cm⁻¹ as an indicator of the extent of EMIm⁺ reorientation. This ratio shows a more rapid increase with the applied potential and reaches a higher value at -2.5 V for 500 mM EMImBF₄ compared with 50 mM and neat EMImBF₄ (Figures 3, S8, and S10). This indicates a more pronounced reorientation of EMIm⁺ cations in 500 mM solution as a function of applied potential, indicating that stronger local electric fields exist in solutions with intermediate ionic concentrations.

We also studied the concentration-dependent behavior of 1-ethyl-2,3-dimethylimidazolium tetrafluoroborate (EMMImBF₄), an ionic liquid that was reported to display higher reactivity than EMImBF₄ at low concentrations due to the methylation of the C2 site that prevents carbene formation.^{14,19,41} We found that solution ion concentration critically determines if methylation enhances or detracts from reactivity. We successfully reproduced the high activity of CO₂ reduction using EMMImBF₄ at a low concentration (25 mM) with a 0.1 M TBA BF₄ supporting electrolyte. However, increasing the concentration of EMMImBF₄ to 125 mM and higher resulted in significantly lower current densities and FEs in 3-hour electrolysis (Figure 4A).

Upon further examination, we found that the CVs associated with higher concentrations of EMMImBF₄ yielded vastly different shapes between the initial and subsequent cycles (Figures S12–S15), unlike EMImBF₄ which maintained the same shape between cycles (Figure S11). Although the initial

cycles for EMMImBF typically yielded current densities greater than -20 mA/cm² and displayed the same non-monotonic enhancement as EMImBF₄ (Figure S16), the following cycles appeared to allow little or no CO₂ electroreduction. Steady-state current densities also showed immediate decrease in current density upon initial polarization, and FEs reached a maximum at 125 mM EMMImBF₄ (Figure 4).

To understand this surprising drop in reactivity, we used *in situ* SERS and optical microscopy to observe electrode surfaces as reactions proceeded. When electrolyte solutions were saturated with CO₂, we observed the potential-dependent nucleation and growth of crystals even when the concentration of EMMImBF was as low as 50 mM (Figures 4B, S18 and S19). Interestingly, similar crystals formed in CO₂-saturated solutions of EMMImBr and EMMImTSFI at potentials close to the onset potential for CO₂ reduction (Figures S20 and S21), suggesting that the crystallization was independent of anion identity and was derived from processes related to CO₂ reduction. Indeed, NMR analysis indicates that the crystals are EMMImHCO₃, which is insoluble in acetonitrile (Figures S22 and S23). Therefore, we deduce that initial CO₂ reduction in EMMImBF₄ electrolytes quickly built up HCO₃⁻ at the electrode–electrolyte interface, which then precipitates with EMMIm cations to rapidly passivate electrode surfaces.

Electrode passivation, along with carbonate or bicarbonate formation, is a major hurdle that must be overcome to achieve efficient CO₂ electroreduction. The onset potential and rate of crystal nucleation and growth varied with the corresponding anion or when we added supporting electrolytes such as TBA BF₄. These changes in the rate of electrode passivation suggest promising pathways toward combating the issue of electrode passivation by disrupting crystal formation via tuning interfacial assembly. Furthermore, these results offer an explanation for the high activity of EMImBF₄⁻, as it is able to form a carboxylate with HCO₃⁻ in solution, decreasing the bicarbonate concentration near the electrode surface. In doing so, EMImBF₄ appears to mitigate the problem of bicarbonate formation to an extent, a pathway that is unavailable to the other ionic liquids we examined.

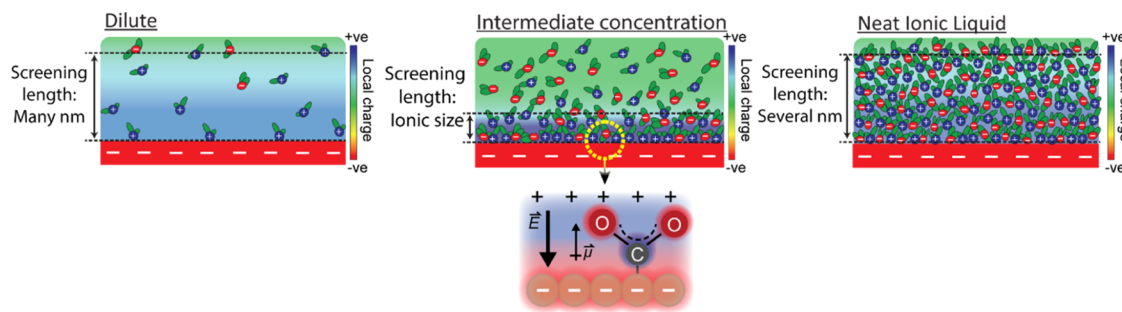


Figure 5. We propose that by changing concentration as a proxy for changing ionic correlations, we can drastically enhance CO_2 electroreduction rates by modulating the double layer thicknesses and electrostatic screening lengths. For dilute and concentrated regimes, a lack of ions and excessive ionic correlations, respectively, induce the formation of thick double layers. At the crossover between the dilute and correlated regimes, intermediate concentrations facilitate the formation of thin double layers, which can screen electrode potentials across molecular-level distances and sustain large gradients in electric field strength. At these intermediate concentrations, the screening length approaches ionic sizes, forming a double layer that is more efficient at electrostatic screening and creating a large potential gradient. This large potential gradient near electrode surfaces would stabilize intermediates and transition states.

DISCUSSION

The general nature of nonmonotonic concentration-dependent reactivity in different ionic liquid-derived electrolytes, together with *in situ* SERS results on EMIm BF_4^- , indicates that differences in CO_2 reduction rates originate from changes in screening efficiency as a nonmonotonic function of ion concentration (Figure 5). To substantiate the plausibility of this mechanism, we performed a mean-field scaling theory analysis of how the Debye screening length for ionic liquid-acetonitrile blends depends on solution concentration. A more detailed discussion of the limitations and implications of the Debye–Hückel theory and our scaling analysis can be found in the Supporting Information.

Briefly, dilute electrolyte theory, such as Debye–Hückel theory, predicts that electrostatic screening lengths, and correspondingly, double layer thicknesses, arise from competition between ion entropy of mixing, which favors thicker double layers, and ion-surface Coulomb interactions that favor thinner double layers. In the dilute limit, the key length scale associated with screening is the Debye screening length, which can be calculated using ion concentration, ion valence, and solution permittivity. With the Debye length as a proxy for the electric double layer thickness, dilute theory predicts that electrostatic screening lengths and double layer thicknesses always decrease, indicating enhanced screening, as ion concentration increases.

Yet, dilute electrolyte theories neglect ion–ion interactions, leading to predicted Debye lengths that become smaller than any plausible dimension of individual ions as concentration is increased (Figure S24). In this limit, ion–ion interactions drive ion clustering into charge-neutral aggregates as the ion concentration is further increased. Cluster formation decreases the concentration of “free ions” available to participate in screening, leading to a disparity between the “free ion” concentration and total number of ions per unit volume. Indeed, recent work on ionic liquid-solvent blends and aqueous electrolytes from the surface forces community indicates that a primary signature of ion–ion correlations is deviation of measured electrostatic screening lengths from the calculated Debye length, which arises at around 1 M.^{25,27}

Taken together, we propose that ionic liquid electrolytes with either dilute or very high ion concentrations can have relatively long screening lengths at the order of several nanometers due to a scarcity of ions and the clustering of ions

to neutral aggregates, respectively, leading to inefficient screening.^{28–30} At intermediate concentrations, the transition between dilute and correlated regimes should yield double layers with much shorter screening lengths, as there are sufficient ions to efficiently screen surface potentials without the presence of excessive impeding ion clusters.

More broadly, thin double layers yield steeper potential gradients as applied potentials are screened within short distances, and the magnitude of the local potential gradient is key in determining electrochemical reaction rates.^{43,58,59} In strongly screening cases, large potential gradients will enhance reactivity by creating polarized environments that require less energy for bonds to bend or break. Similar themes of electric field gradients enhancing reactivity are found in biology, where potential gradients in enzyme active sites orient and break chemical bonds or stabilize important reaction intermediates.^{58–61}

In CO_2 electroreduction, a key intermediate is $\text{CO}_2^{\bullet-}$, an unstable and bent negative radical with a permanent dipole. Therefore, a compact and strongly screening double layer achieved at intermediate concentrations would more effectively stabilize $\text{CO}_2^{\bullet-}$, leading to the maximum rate of CO_2 electroreduction. In contrast, electrolytes in dilute and correlated regimes, where ionic screening lengths are longer, would be expected to form an environment that is less amenable to stabilizing charged or polar intermediates and lead to lower reactivity.

Overall, our scaling theory analysis links the regime of highest expected reactivity with that of the most efficient double layer screening and suggests that intermediate ion concentration may be a generally advantageous electrolyte regime for electrocatalytic processes. Yet, we caution that the electric double layer is a dynamic and complex environment during electrochemical reactions that cannot be comprehensively described using classical electrolyte theory, especially at high ionic liquid concentrations where ionic liquid assembly plays a major role.⁶² Future refinement of the proposed mechanism would require new ways of measuring electrolyte structure and potential distributions at interfaces, molecular dynamics simulations, or other approaches that yield further molecular details on the role of ionic correlations.

Our interpretation explains the concentration-dependent reactivity trend we observe, where reaction rates are non-monotonic with ion concentration. In particular, intermediate

concentrations create local reaction environments that better facilitate the formation of intermediates and turnover to products. Importantly, this characteristic of compact and thin double layers is not restricted to only cocatalytic ionic liquids, as evidenced by the EMPyrr BF_4^- studies. We anticipate that our findings have applications extending far beyond CO_2 electroreduction and may prove useful in both understanding, as well as controlling energy-intensive electrochemical reactions such as nitrogen fixation.

CONCLUSIONS AND FUTURE WORK

In this work, we show that ionic liquid-based electrolytes exhibit pronounced nonmonotonic reactivity-concentration scaling for electrochemical CO_2 reduction to CO. Our conclusions are supported by CV studies of reaction kinetics as well as steady-state electrolysis experiments. Notably, our findings are general for multiple classes of ionic liquids and should also extend to other solvents.

To substantiate our conclusions, we performed SERS and found that more strongly screening environments were formed near electrode surfaces at intermediate concentrations, where we observed higher reactivity. This is evidenced by more pronounced changes to potential-dependent ring deformation at intermediate concentrations, observed as shifts in the Raman scattering exhibited by the imidazolium ring structure.

We interpret our data set to indicate that electrostatic screening is more efficient at intermediate concentrations, leading to thinner electric double layers, which facilitate CO_2 reduction via near-surface localization of potential gradients. While EMMIm BF_4^- does exhibit a nonmonotonic concentration-reactivity trend based on CV data, CA measurements are hindered by precipitation of an insulating crystalline layer over time, which inhibits further CO_2 electrochemical reduction. We determined that this crystalline precipitate occurs due to the formation of HCO_3^- species, which drive the nucleation and growth of a crystalline insulating EMMIm HCO_3^- film under reaction conditions. This important result suggests that the EMIm BF_4^- reactivity is partially owed to the ability of the C2 position to coordinate HCO_3^- and also offers potential strategies to combat electrode passivation.

In summary, our findings have important implications for understanding how tuning electric double layer assembly, and in turn, local reaction environments, could enhance or enable better control over reactivity in important electrochemical reactions. We show that tuning electric double layer screening efficiency can significantly influence the electrocatalytic reaction both in terms of current density and faradaic efficiency. Our preliminary scaling analysis suggests that the Debye screening length can be a simple and useful metric for analyzing screening efficiency by showing that the range of concentrations in which the Debye screening length approaches ion sizes is an ideal regime to explore for enhanced reactivity. Notably, our proposed theory is not ion- or solvent-specific and can be generalized to electrochemical processes requiring different electrolyte compositions or more energy-intensive electrocatalytic reactions. Our findings show that the liquid side of electrode–electrolyte interfaces can be used to sculpt reaction landscapes in ways that can rival the influence of the solid side of electrochemical interfaces.

EXPERIMENTAL DETAILS

Chemicals. The ionic liquids used in the preparation of the electrolytes were 1-ethyl-3-methylimidazolium tetrafluoroborate (EMIm BF_4^- , >98% purity, Iolitec), 1-ethyl-2,3-dimethylimidazolium tetrafluoroborate (EMMIm BF_4^- , 97% purity, Alfa Aesar), 1-ethyl-1-methylpyrrolidinium tetrafluoroborate (EMPyrr BF_4^- , >98% purity, Iolitec), and tetrabutylammonium tetrafluoroborate (TBA BF_4^- , 99% purity, Sigma-Aldrich). All ionic liquids were used without further purification. NMR and electrochemical analysis were used to confirm purity upon receiving the chemicals. Ultrapure water (Milli-Q, $\geq 18.2 \text{ M}\Omega\text{cm}$) was used in all experiments. HPLC-grade acetonitrile and ethanol were purchased from Fisher Chemicals and Decon Labs. Inc., respectively. Deuterated dimethylsulfoxide (DMSO-d6) was from Sigma-Aldrich. CO_2 and Ar gas were purchased from Airgas. In the synthesis of Ag nanoparticles, silver nitrate was from Alfa Aesar, sodium borohydride was from Sigma-Aldrich, and sodium citrate dihydrate was from Fisher Bioreagents.

Electrochemical Methods. Electrochemical measurements were performed in borosilicate glass cells and were carried out using a BioLogic VSP potentiostat. Electrolyte solutions were composed of ionic liquids dissolved in acetonitrile. Because of the hygroscopic nature of acetonitrile, water content of stock acetonitrile ranged from <100 ppm to 500 ppm. Water is a potential source of protons for CO_2 electroreduction, so water content is known to impact observed reactivity. To control the influence of trace water, water was systematically added to the acetonitrile to reach concentrations of 900–1100 ppm to maintain consistent electrolyte conditions between trials. In parallel experiments, we undertook extensive efforts to dry all electrolyte materials and found that CO_2 reduction is suppressed in extensively dried ionic liquid-based electrolytes, consistent with literature reports.^{4,63,64} Hence, water is an essential proton source during ionic liquid-mediated CO_2 reduction, and our results substantiate this conclusion, as elaborated in Results and Discussion.

Measurements of water content were carried out using a Mettler Toledo C10S Coulometric Karl Fischer Titrator. For CV and CA measurements, the working electrode was a polycrystalline Ag electrode (BASi) with a geometric surface area of 0.071 cm^2 . All current densities presented in this work are normalized to the geometric surface area. The working electrodes were polished to a mirror finish based on established protocols using 15, 3, and $1 \mu\text{m}$ diamond polish and then $0.05 \mu\text{m}$ alumina (BASi) to a mirror finish prior to sonication to remove adsorbed alumina. Quantitative agreement with prior studies was achieved using this method. For all electrochemical measurements, we used an Ag/Ag^+ nonaqueous reference electrode and a coiled platinum wire as a counter electrode. A ferrocene/ferrocenium redox couple was used initially to confirm the applicability of an Ag/Ag^+ (0.01 M AgNO_3) nonaqueous reference previously described for acetonitrile-containing electrolytes. Because the silver surface readily oxidizes in the potential range near the ferrocene/ferrocenium redox couple, all potentials used in this work are referenced to the Ag/Ag^+ (0.01 M AgNO_3) reference.⁴⁶ Electrolyte solutions were purged for 20 min prior to electrochemical measurements using either Ar or CO_2 gas.

For CV measurements, we designed and 3D-printed caps using a chlorinated polyethylene elastomer filament (Prusa) for

the one-compartment batch electrochemical cell to ensure reproducible cell geometry and to control for effects of solution resistance across trials. All CV measurements were carried out at scan rates of 100 mV/s.

Product Analysis. We studied the products of electrolysis and determined corresponding faradaic efficiencies using a custom-made gas-tight two-compartment cell in CA studies. The compartments were separated using a Nafion 117 membrane and were continuously stirred as well as purged with CO₂. The compartments were well mixed to eliminate transport effects (Figure S25). Potentials of -2.5 V were held for 3 h, where the steady state was reached after 1 h.

Nafion 117 membranes for CA studies were prepared according to the literature prior to use.^{19,65,66} In brief, as-received membranes precut to desired dimensions were immersed in 3 wt % H₂O₂ aqueous solution, Milli-Q Ultrapure water, 1 M H₂SO₄ aqueous solution, and Milli-Q Ultrapure water again in sequence. All solutions were heated to 80 °C, and each step took 1 h. After preparation, we stored membranes in 0.1 M TBA BF₄-acetonitrile solution when not in use, and the membranes were rinsed with Milli-Q Ultrapure water and acetonitrile every time prior to use.

Gaseous products of CA experiments were analyzed every 20 min using a gas chromatograph (SRI Multiple Gas Analyzer #5) with a thermal conductivity detector (TCD) and a flame-ionization detector (FID) equipped with a methanizer. A HayeSep D column was connected to the TCD while the FID was connected to a HayeSep D and a Molesieve 5A column (Restek). Ultrahigh-purity grade He (Airgas) was used as the carrier gas.

The faradaic efficiency was calculated by:⁶⁷

$$FE (\%) = \frac{\frac{\nu}{60 \text{ s} / \text{min}} \times \frac{y}{24,000 \text{ cm}^3 / \text{mol}} \times N \times F}{i} \times 100\%$$

where ν = 9.2 sccm is the flow rate of CO₂, y is the concentration of product measured from GC in the unit of mole fraction, N = 2 is the number of electrons consumed to convert one CO₂ molecule to one CO, F = 96,500 C mol⁻¹ is the Faraday constant, and i is the total current passing through the working electrode in the unit of A.

We performed NMR spectroscopy using a 400 MHz NMR spectrometer (Bruker Avance) with a BBFO probe to evaluate the electrolyte composition before and after CA experiments through ¹H NMR and ¹³C NMR. DMSO-d6 was used as the solvent.

SERS Measurements. Electrochemical SERS measurements were carried out using a single-compartment PTFE electrochemical cell with a polished L-shaped Ag working electrode (Shanghai Fanyue Electronic Technology Co. Ltd.) prepared by drop-casting Ag nanoparticles onto the surface to achieve enhancement. Ag nanoparticles were synthesized based on a previously reported method.⁶⁸ The counter electrode was a polished and coiled Pt wire, while the reference electrode was a nonaqueous Ag/Ag⁺ (0.01 M AgNO₃) reference. The electrolyte was purged with either Ar or CO₂ for 20 min prior to conducting the measurements. SERS spectra were collected using a Thermo-Fisher Scientific DXRxi Raman Imaging Microscope with a 532 nm excitation laser and at 10x magnification. The laser power was 9.0 mW, and the acquisition time was 0.033 s (30 Hz) with 300 scans for all measurements. Potential-dependent SERS spectra were collected by sweeping the potential from -0.7 to -2.5 V

and then back to -0.7 V. Optical images of the working electrode surface were also captured using the same Raman imaging microscope in video mode.

ASSOCIATED CONTENT

Supporting Information

The Supporting Information is available free of charge at <https://pubs.acs.org/doi/10.1021/acscatal.2c02154>.

Further discussion of scaling theory and additional experimental data (PDF)

AUTHOR INFORMATION

Corresponding Author

Matthew A. Gebbie – Department of Chemical and Biological Engineering, University of Wisconsin–Madison, Madison, Wisconsin 53706, United States;  orcid.org/0000-0002-4619-4002; Email: gebbie@wisc.edu

Authors

Beichen Liu – Department of Chemical and Biological Engineering, University of Wisconsin–Madison, Madison, Wisconsin 53706, United States

Wenxiao Guo – Department of Chemical and Biological Engineering, University of Wisconsin–Madison, Madison, Wisconsin 53706, United States;  orcid.org/0000-0002-6674-9714

Complete contact information is available at:

<https://pubs.acs.org/10.1021/acscatal.2c02154>

Author Contributions

The manuscript was written through contributions of all authors. All authors have given approval to the final version of the manuscript.

Funding

The authors acknowledge support from the Department of Chemical and Biological Engineering at the University of Wisconsin–Madison and the Wisconsin Alumni Research Fund. M.A.G. acknowledges support from the Michael F. and Virginia H. Conway Assistant Professorship. B.L. acknowledges support from the Fenton-May Graduate Fellowship.

Notes

The authors declare no competing financial interest.

ACKNOWLEDGMENTS

This work used facilities and instrumentation at the UW-Madison Wisconsin Centers for Nanoscale Technology (wcnt.wisc.edu) partially supported by the NSF through the University of Wisconsin Materials Research Science and Engineering Center (DMR-1720415). The Bruker AVANCE 400 NMR spectrometer was supported by NSF grant CHE-1048642.

REFERENCES

- (1) Chandrasekaran, K.; Bockris, J. O. M. In-situ spectroscopic investigation of adsorbed intermediate radicals in electrochemical reactions – CO₂^{·-}. *Surf. Sci.* **1987**, *185*, 495–514.
- (2) Hori, Y.; Wakebe, H.; Tsukamoto, T.; Koga, O. Electrocatalytic process of CO selectivity in electrochemical reduction of CO₂ at metal electrodes in aqueous media. *Electrochim. Acta* **1993**, *94*, 1833–1839.
- (3) Rosen; Salehi-Khojin, A.; Thorson, M. R.; Zhu, W.; Whipple, D. T.; Kenis, P. J. A.; Masel, R. I. Ionic Liquid–Mediated Selective

- Conversion of CO₂ to CO at Low Overpotentials. *Science* **2011**, *334*, 643.
- (4) Rosen, B. A.; Zhu, W.; Kaul, G.; Salehi-Khojin, A.; Masel, R. I. Water Enhancement of CO₂ Conversion on Silver in 1-Ethyl-3-Methylimidazolium Tetrafluoroborate. *J. Electrochem. Soc.* **2012**, *160*, H138–H141.
- (5) Bondue, C. J.; Graf, M.; Goyal, A.; Koper, M. T. M. Suppression of Hydrogen Evolution in Acidic Electrolytes by Electrochemical CO₂ Reduction. *J. Am. Chem. Soc.* **2021**, *143*, 279–285.
- (6) Rosen, B. A.; Haan, J. L.; Mukherjee, P.; Braunschweig, B.; Zhu, W.; Salehi-Khojin, A.; Dlott, D. D.; Masel, R. I. In Situ Spectroscopic Examination of a Low Overpotential Pathway for Carbon Dioxide Conversion to Carbon Monoxide. *J. Phys. Chem. C* **2012**, *116*, 15307–15312.
- (7) Wang, Y.; Hayashi, T.; He, D.; Li, Y.; Jin, F.; Nakamura, R. A reduced imidazolium cation layer serves as the active site for electrochemical carbon dioxide reduction. *Appl. Catal., B* **2020**, *264*, No. 118495.
- (8) Faggion, D., Jr.; Goncalves, W. D. G.; Dupont, J. CO₂ Electroreduction in Ionic Liquids. *Front. Chem.* **2019**, *7*, 102.
- (9) Appel, A. M.; Bercaw, J. E.; Bocarsly, A. B.; Dobbek, H.; DuBois, D. L.; Dupuis, M.; Ferry, J. G.; Fujita, E.; Hille, R.; Kenis, P. J.; Kerfel, C. A.; Morris, R. H.; Peden, C. H. F.; Portis, A. R.; Ragsdale, S. W.; Rauchfuss, T. B.; Reek, J. N. H.; Seefeldt, L. C.; Thauer, R. K.; Waldrop, G. L. Frontiers, opportunities, and challenges in biochemical and chemical catalysis of CO₂ fixation. *Chem. Rev.* **2013**, *113*, 6621–6658.
- (10) Alvarez-Guerra, M.; Albo, J.; Alvarez-Guerra, E.; Irabien, A. Ionic liquids in the electrochemical valorisation of CO₂. *Energy Environ. Sci.* **2015**, *8*, 2574–2599.
- (11) Welton, T. Ionic liquids: a brief history. *Biophys. Rev.* **2018**, *10*, 691–706.
- (12) Rogers, R. D.; Seddon, K. R. Ionic Liquids—Solvents of the Future? *Science* **2003**, *302*, 792–793.
- (13) Sheldon, R. Catalytic reactions in ionic liquids. *Chem. Commun.* **2001**, *23*, 2399–2407.
- (14) Lau, G. P. S.; Schreier, M.; Vasilyev, D.; Scopelliti, R.; Gratzel, M.; Dyson, P. J. New Insights Into the Role of Imidazolium-Based Promoters for the Electroreduction of CO₂ on a Silver Electrode. *J. Am. Chem. Soc.* **2016**, *138*, 7820–7823.
- (15) Ratschmeier, B.; Braunschweig, B. Cations of Ionic Liquid Electrolytes Can Act as a Promoter for CO₂ Electrocatalysis through Reactive Intermediates and Electrostatic Stabilization. *J. Phys. Chem. C* **2021**, *125*, 16498–16507.
- (16) Wang, Y.; Hatakeyama, M.; Ogata, K.; Wakabayashi, M.; Jin, F.; Nakamura, S. Activation of CO₂ by ionic liquid EMIM-BF₄ in the electrochemical system: a theoretical study. *Phys. Chem. Chem. Phys.* **2015**, *17*, 23521–23531.
- (17) Vasilyev, D. V.; Shyshkanov, S.; Shirzadi, E.; Katsyuba, S. A.; Nazeeruddin, M. K.; Dyson, P. J. Principal Descriptors of Ionic Liquid Co-catalysts for the Electrochemical Reduction of CO₂. *ACS Appl. Energy Mater.* **2020**, *3*, 4690–4698.
- (18) Dupont, J.; Simon, N. M.; Zanatta, M. The Nature of Carbon Dioxide in Bare Ionic Liquids. *ChemSusChem* **2020**, *13*, 3101–3109.
- (19) Sun, L. Y.; Ramesha, G. K.; Kamat, P. V.; Brennecke, J. F. Switching the Reaction Course of Electrochemical CO₂ Reduction with Ionic Liquids. *Langmuir* **2014**, *30*, 6302–6308.
- (20) Gu, L. Z.; Zhang, Y. Unexpected CO₂ Splitting Reactions To Form CO with N-Heterocyclic Carbenes as Organocatalysts and Aromatic Aldehydes as Oxygen Acceptors. *J. Am. Chem. Soc.* **2010**, *132*, 914–915.
- (21) Noack, K.; Schulz, P. S.; Paape, N.; Kiefer, J.; Wasserscheid, P.; Leipertz, A. The role of the C2 position in interionic interactions of imidazolium based ionic liquids: a vibrational and NMR spectroscopic study. *Phys. Chem. Chem. Phys.* **2010**, *12*, 14153–14161.
- (22) Whipple, D. T.; Kenis, P. J. A. Prospects of CO₂ Utilization via Direct Heterogeneous Electrochemical Reduction. *J. Phys. Chem. Lett.* **2010**, *1*, 3451–3458.
- (23) Kemna, A.; Braunschweig, B. Potential-Induced Adsorption and Structuring of Water at the Pt(111) Electrode Surface in Contact with an Ionic Liquid. *J. Phys. Chem. Lett.* **2020**, *11*, 7116–7121.
- (24) König, M.; Vaes, J.; Klemm, E.; Pant, D. Solvents and Supporting Electrolytes in the Electrocatalytic Reduction of CO₂. *iScience* **2019**, *19*, 135–160.
- (25) Smith, A. M.; Lee, A. A.; Perkin, S. The Electrostatic Screening Length in Concentrated Electrolytes Increases with Concentration. *J. Phys. Chem. Lett.* **2016**, *7*, 2157–2163.
- (26) Gebbie, M. A.; Valtiner, M.; Banquy, X.; Fox, E. T.; Henderson, W. A.; Israelachvili, J. N. Ionic liquids behave as dilute electrolyte solutions. *Proc. Natl. Acad. Sci. U. S. A.* **2013**, *110*, 9674–9679.
- (27) Gebbie, M. A.; Smith, A. M.; Dobbs, H. A.; Lee, A. A.; Warr, G. G.; Banquy, X.; Valtiner, M.; Rutland, M. W.; Israelachvili, J. N.; Perkin, S.; Atkin, R. Long range electrostatic forces in ionic liquids. *Chem. Commun.* **2017**, *53*, 1214–1224.
- (28) Bazant, M. Z.; Storey, B. D.; Kornyshev, A. A. Double layer in ionic liquids: overscreening versus crowding. *Phys. Rev. Lett.* **2011**, *109*, 149903.
- (29) Kornyshev, A. A. Double-Layer in Ionic Liquids: Paradigm Change? *J. Phys. Chem. B* **2007**, *111*, 5545–5557.
- (30) Lee, A. A.; Perez-Martinez, C. S.; Smith, A. M.; Perkin, S. Scaling Analysis of the Screening Length in Concentrated Electrolytes. *Phys. Rev. Lett.* **2017**, *119*, No. 026002.
- (31) de Souza, J. P.; Bazant, M. Z. Continuum Theory of Electrostatic Correlations at Charged Surfaces. *J. Phys. Chem. C* **2020**, *124*, 11414–11421.
- (32) Gebbie, M. A.; Dobbs, H. A.; Valtiner, M.; Israelachvili, J. N. Long-range electrostatic screening in ionic liquids. *Proc. Natl. Acad. Sci. U. S. A.* **2015**, *112*, 7432–7437.
- (33) Han, M.; Kim, H.; Leal, C.; Negrito, M.; Batteas, J. D.; Espinosa-Marzal, R. M. Insight into the Electrical Double Layer of Ionic Liquids Revealed through Its Temporal Evolution. *Adv. Mater. Interfaces* **2020**, *7*, No. 2001313.
- (34) García Rey, N.; Dlott, D. D. Structural Transition in an Ionic Liquid Controls CO₂ Electrochemical Reduction. *J. Phys. Chem. C* **2015**, *119*, 20892–20899.
- (35) Lim, H.-K.; Kwon, Y.; Kim, H. S.; Jeon, J.; Kim, Y.-H.; Lim, J.-A.; Kim, B.-S.; Choi, J.; Kim, H. Insight into the Microenvironments of the Metal–Ionic Liquid Interface during Electrochemical CO₂ Reduction. *ACS Catal.* **2018**, *8*, 2420–2427.
- (36) Hahn, C.; Jaramillo, T. F. Using Microenvironments to Control Reactivity in CO₂ Electrocatalysis. *Joule* **2020**, *4*, 292–294.
- (37) Hansen, K. U.; Jiao, F. Creating the right environment. *Nat. Energy* **2021**, *6*, 1005–1006.
- (38) Kim, C.; Bui, J. C.; Luo, X.; Cooper, J. K.; Kusoglu, A.; Weber, A. Z.; Bell, A. T. Tailored catalyst microenvironments for CO₂ electroreduction to multicarbon products on copper using bilayer ionomer coatings. *Nat. Energy* **2021**, *6*, 1026–1034.
- (39) Zhao, S.-F.; Horne, M.; Bond, A. M.; Zhang, J. Is the Imidazolium Cation a Unique Promoter for Electrocatalytic Reduction of Carbon Dioxide? *J. Phys. Chem. C* **2016**, *120*, 23989–24001.
- (40) Tanner, E. E. L.; Batchelor-McAuley, C.; Compton, R. G. Carbon Dioxide Reduction in Room-Temperature Ionic Liquids: The Effect of the Choice of Electrode Material, Cation, and Anion. *J. Phys. Chem. C* **2016**, *120*, 26442–26447.
- (41) Vasilyev, D. V.; Dyson, P. J. The Role of Organic Promoters in the Electroreduction of Carbon Dioxide. *ACS Catal.* **2021**, *11*, 1392–1405.
- (42) Bard, A. J.; Faulkner, L. R. *Electrochemical Methods: Fundamentals and Applications*; 2nd ed.; Wiley, 2001; pp 23–28, 251–252, 417–418, 648–650.
- (43) Gu, J.; Liu, S.; Ni, W.; Ren, W.; Haussener, S.; Hu, X. Modulating electric field distribution by alkali cations for CO₂ electroreduction in strongly acidic medium. *Nat. Catal.* **2022**, *5*, 268.
- (44) Monteiro, M. C. O.; Dattila, F.; Lopez, N.; Koper, M. T. M. The Role of Cation Acidity on the Competition between Hydrogen

- Evolution and CO₂ Reduction on Gold Electrodes. *J. Am. Chem. Soc.* **2022**, *144*, 1589–1602.
- (45) Marcandalli, G.; Goyal, A.; Koper, M. T. M. Electrolyte effects on the faradaic efficiency of CO₂ reduction to CO on a gold electrode. *ACS Catal.* **2021**, *11*, 4936–4945.
- (46) Pavlishchuk, V. V.; Addison, A. W. Conversion constants for redox potentials measured versus different reference electrodes in acetonitrile solutions at 25 °C. *Inorg. Chim. Acta* **1999**, *298*, 97–102.
- (47) Matsubara, Y.; Grills, D. C.; Kuwahara, Y. Thermodynamic Aspects of Electrocatalytic CO₂ Reduction in Acetonitrile and with an Ionic Liquid as Solvent or Electrolyte. *ACS Catal.* **2015**, *5*, 6440–6452.
- (48) Santos, V. O.; Leite, I. R.; Brolo, A. G.; Rubim, J. C. The electrochemical reduction of CO₂ on a copper electrode in 1-n-butyl-3-methyl imidazolium tetrafluoroborate (BMI.BF₄) monitored by surface-enhanced Raman scattering (SERS). *J. Raman Spectrosc.* **2016**, *47*, 674–680.
- (49) Michez, R.; Doneux, T.; Buess-Herman, C.; Luhmer, M. NMR Study of the Reductive Decomposition of [BMIm][NTf₂] at Gold Electrodes and Indirect Electrochemical Conversion of CO₂. *ChemPhysChem* **2017**, *18*, 2208–2216.
- (50) Monteiro, M. C. O.; Philips, M. F.; Schouten, K. J. P.; Koper, M. T. M. Efficiency and selectivity of CO₂ reduction to CO on gold gas diffusion electrodes in acidic media. *Nat. Commun.* **2021**, *12*, 4943.
- (51) Li, T.; Lees, E. W.; Goldman, M.; Salvatore, D. A.; Weekes, D. M.; Berlinguet, C. P. Electrolytic Conversion of Bicarbonate into CO in a Flow Cell. *Joule* **2019**, *3*, 1487–1497.
- (52) Rabinowitz, J. A.; Kanan, M. W. The future of low-temperature carbon dioxide electrolysis depends on solving one basic problem. *Nat. Commun.* **2020**, *11*, 5231.
- (53) Foley, J.; Korzeniewski, C.; Pons, S. Anodic and cathodic reactions in acetonitrile/tetra- n -butylammonium tetrafluoroborate: an electrochemical and infrared spectroelectrochemical study. *Can. J. Chem.* **1988**, *66*, 201–206.
- (54) Berto, T. C.; Zhang, L.; Hamers, R. J.; Berry, J. F. Electrolyte Dependence of CO₂ Electroreduction: Tetraalkylammonium Ions Are Not Electrocatalysts. *ACS Catal.* **2014**, *5*, 703–707.
- (55) Dhumal, N. R.; Noack, K.; Kiefer, J.; Kim, H. J. Molecular Structure and Interactions in the Ionic Liquid 1-Ethyl-3-methylimidazolium Bis(Trifluoromethylsulfonyl)imide. *J. Phys. Chem. A* **2014**, *118*, 2547–2557.
- (56) Sanchora, P.; Pandey, D. K.; Rana, D.; Materny, A.; Singh, D. K. Impact of Size and Electronegativity of Halide Anions on Hydrogen Bonds and Properties of 1-Ethyl-3-methylimidazolium-Based Ionic Liquids. *J. Phys. Chem. A* **2019**, *123*, 4948–4963.
- (57) Santos, V. O.; Alves, M. B.; Carvalho, M. S.; Suarez, P. A. Z.; Rubim, J. C. Surface-Enhanced Raman Scattering at the Silver Electrode/Ionic Liquid (BMIPF₆) Interface. *J. Phys. Chem. B* **2006**, *110*, 20379–20385.
- (58) Siddiqui, S. A.; Dubey, K. D. Can the local electric field be a descriptor of catalytic activity? A case study on chorismate mutase. *Phys. Chem. Chem. Phys.* **2021**, *24*, 1974–1981.
- (59) Léonard, N. G.; Dhaoui, R.; Chantarojsiri, T.; Yang, J. Y. Electric Fields in Catalysis: From Enzymes to Molecular Catalysts. *ACS Catal.* **2021**, *11*, 10923–10932.
- (60) Resasco, J.; Chen, L. D.; Clark, E.; Tsai, C.; Hahn, C.; Jaramillo, T. F.; Chan, K.; Bell, A. T. Promoter Effects of Alkali Metal Cations on the Electrochemical Reduction of Carbon Dioxide. *J. Am. Chem. Soc.* **2017**, *139*, 11277–11287.
- (61) Lee, G.; Li, Y. C.; Kim, J.-Y.; Peng, T.; Nam, D.-H.; Sedighian Rasouli, A.; Li, F.; Luo, M.; Ip, A. H.; Joo, Y.-C.; Sargent, E. H. Electrochemical upgrade of CO₂ from amine capture solution. *Nat. Energy* **2020**, *6*, 1–8.
- (62) Fedorov, M. V.; Kornyshev, A. A. Ionic liquids at electrified interfaces. *Chem. Rev.* **2014**, *114*, 2978–3036.
- (63) Rudnev, A. V.; Zhumaev, U. E.; Kuzume, A.; Vesztergom, S.; Furrer, J.; Broekmann, P.; Wandlowski, T. The promoting effect of water on the electroreduction of CO₂ in acetonitrile. *Electrochim. Acta* **2016**, *189*, 38–44.
- (64) Figueiredo, M. C.; Ledezma-Yanez, I.; Koper, M. T. M. In Situ Spectroscopic Study of CO₂ Electroreduction at Copper Electrodes in Acetonitrile. *ACS Catal.* **2016**, *6*, 2382–2392.
- (65) Chae, K. J.; Choi, M.; Ajayi, F. F.; Park, W.; Chang, I. S.; Kim, I. S. Mass Transport through a Proton Exchange Membrane (Nafion) in Microbial Fuel Cells. *Energy Fuels* **2008**, *22*, 169–176.
- (66) Sheng, H.; Hermes, E. D.; Yang, X.; Ying, D.; Janes, A. N.; Li, W.; Schmidt, J. R.; Jin, S. Electrocatalytic Production of H₂O₂ by Selective Oxygen Reduction Using Earth-Abundant Cobalt Pyrite (CoS₂). *ACS Catal.* **2019**, *9*, 8433–8442.
- (67) Han, N.; Wang, Y.; Yang, H.; Deng, J.; Wu, J.; Li, Y.; Li, Y. Ultrathin bismuth nanosheets from in situ topotactic transformation for selective electrocatalytic CO₂ reduction to formate. *Nat. Commun.* **2018**, *9*, 1320.
- (68) Agnihotri, S.; Mukherji, S.; Mukherji, S. Size-controlled silver nanoparticles synthesized over the range 5–100 nm using the same protocol and their antibacterial efficacy. *RSC Adv.* **2014**, *4*, 3974–3983.



CAS BIOFINDER DISCOVERY PLATFORM™

CAS BIOFINDER
HELPS YOU FIND
YOUR NEXT
BREAKTHROUGH
FASTER

Navigate pathways, targets, and diseases with precision

Explore CAS BioFinder

